Rubber part characterisation for rotordynamics analysis.

Florian Tezenas Du Montcel, Sébastien Baguet, Marie-Ange Andrianoely, Régis Dufour, Stéphane Grange, L. Briancon, Piotr Kanty

Rubber part characterization for a vibroflot analysis

Florian TEZENAS DU MONTCEL[1,3], Sébastien BAGUET[1], Marie-Ange ANDRIANOELY[1], Régis DUFOUR[1], Stéphane GRANGE[2], Laurent BRIANÇON[2], Piotr KANTY[3]

[1]Univ Lyon, INSA Lyon, CNRS, LaMCoS, UMR5259, F-69621 Villeurbanne, France
[2]Univ Lyon, INSA-Lyon, GEOMAS, EA7495, F-69621 Villeurbanne, France
[3]Menard, 22 rue Jean Rostand, 91400 Orsay, France
florian.tezenas-du-montcel@menard-mail.com

Abstract

This paper presents a method to determine stiffness dynamic characteristic of rubber parts which are used for vibration isolation. The study was motivated by the need of such characteristics to model vibroflot's dynamic behaviour. Vibroflots are used by ground improvement companies to deeply densify sandy soils by vibrations in order to make stable future infrastructures. A classical vibroflot is a slender structure hung from a crane with several extension tubes and cables. The vibroflot is composed of a non-rotating tube casing in contact with the soil, containing a mass unbalanced rotor mounted on rolling bearings driven by an asynchronous electrical motor that produces orbital vibration and therefore the soil compaction. In order to avoid the vibrations to propagate to the extension tubes two big rubber coupling parts are used.

The method presented here is based on five steps. The first step aims at determining material properties and at presenting the hyper-elastic and viscoelastic models used. Then real dynamic tests are carried out on one type of rubber coupling, at different frequencies and dynamic amplitudes, using a hydraulic shaker capable to develop a force up to 62 kN.

Then Finite Elements simulations are conducted to validate material models and parameters on the first geometry. Once the results are satisfactory, simulations are made on the second rubber coupling made of the same material.

Finally, both rubber parts stiffness properties are known for different sets of parameters and can be introduced into the global Finite Elements multi-rotors model for investigating operational runs.

1 Introduction

Vibro compaction is a ground improvement technique which aims to deeply densify sandy soil by vibrations in order to make stable future infrastructure without using concrete [1]. It is executed using a rig (excavator, drilling rig or crane), a vibroflot, and auxiliary equipment such as generator, compressor, and water pumps. Since the development of vibro compaction during the 1930s vibroflots were progressively improved following operational experiences. The current design can be described as a multirotor system driven by an electrical motor (see Figure 1). A non-rotating tube casing, in contact with the soil, involved an eccentric rotor-ball bearing system driven by an electrical motor, produces orbital vibrations. The two rubber couplings hanging the tube casing to the extension tubes, themselves attached to the crane cables, also play the role of damper in order to mitigate the vibration propagation

It appears now necessary for soil improvement companies to accurately model this system to better know and improve their vibro compaction equipment and processes [2]. To do so it is necessary to access rubber coupling parts radial dynamics properties, which are not currently known.

This paper presents a method to determine the stiffness properties of the two rubber couplings having two different geometries but using the same elastomer material. At first the elastomer material is characterised for fitting the parameters of a model combining hyper-elastic and viscoelastic laws. Then dynamic tests are carried

out on the first rubber coupling for different sinus deflection amplitudes and forcing frequencies. The corresponding FE model is developed with Abaqus software by using 3D-solid elements. The comparison of the calculated and measured force - deflection loops has the objective to validate experimentally the elastomer model for applying it to the second rubber coupling. Once the predicted stiffnesses are determined versus the forcing parameters, they are introduced in the developed Finite Elements model coupling the rotordynamics and the sandy soil.

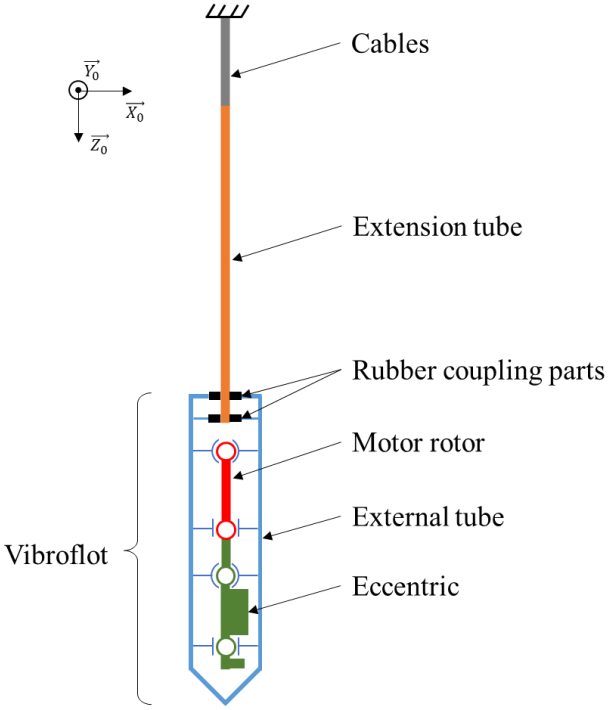

Figure 1: Vibroflot sketch.

2 Rubber characterisation

2.1 Context

To access rubber material properties uniaxial tests were carried out on elastomer samples (length ~ 13.5 mm; width ~ 4.0 mm; thickness ~ 1.3 mm) under tension using a Dynamic Mechanical Analysis (DMA) machine, in a quasi-static way – to calibrate the hyper elastic model – and in a dynamic way – to calibrate the viscoelastic model.

2.2 Hyper elasticity

To calibrate the hyper elastic model, quasi-static tests were performed at two different temperatures, which are the minimum and maximum temperatures measured while the rubber coupling are operating. Hyper-elastic laws are usually used to predict behaviours at tens or hundreds of percentages of strain [3]. In this case the strain is quite small (see Figure 2), but we will use this kind of non-linear law to reproduce the stiffening observed at small strain.

Among the different hyper-elastic models available the Mooney-Rivlin model is used. It's a good compromise between the Neo-Hooke model, which is too much linear, and the other ones which are more complex [4]. The strain energy density function is:

$$U = C_{10}(\bar{I}_1 - 3) + C_{01}(\bar{I}_2 - 3) + \frac{1}{D_1}\left(J^{el} - 1\right)^2 \quad (1)$$

Where C_{10}, C_{01}, and D_1 are temperature-dependent material constants, $\bar{I}_1$, $\bar{I}_2$, are the first and second deviatoric strain invariant and J^{el} is the elastic volume ratio.

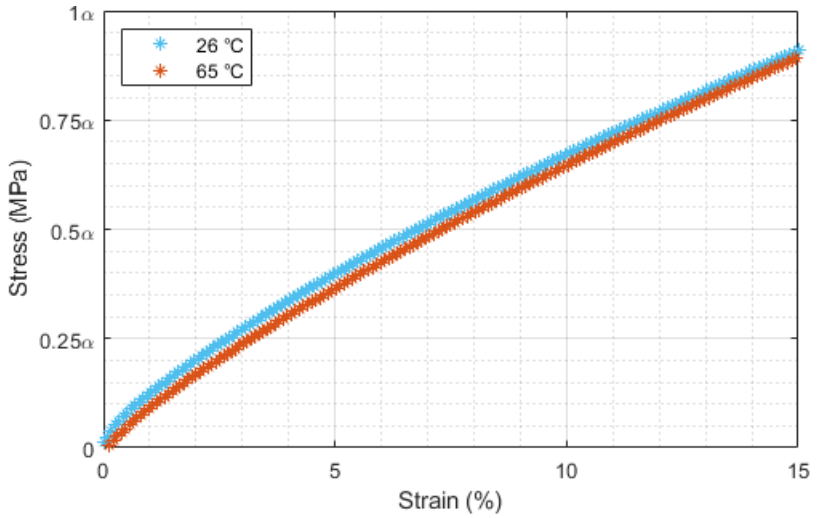

Figure 2: Uniaxial tension stress-strain curves obtained at 26°C and 65°C.

To obtain material constants a curve fitting algorithm is used with the uniaxial tension tests at 26°C and 65°C as input data [5]. The Poisson's ratio is set at 0.495. The results are summarized in Table 1.

Temperature	C_{10} (MPa)	C_{01} (MPa)	D_1 (MPa^{-1})
26 °C	-2.45 η	3.59 η	0.0045 η
65 °C	-0.83 η	1.76 η	0.0055 η

Table 1: Mooney-Rivlin parameters identified for two temperatures between 0% and 15% of strain.

2.3 Viscoelasticity

To calibrate the viscoelastic model, dynamic tests were performed at small strain (0.05%), but for different frequencies and temperatures. The results are typical and plotted in Figure 3.

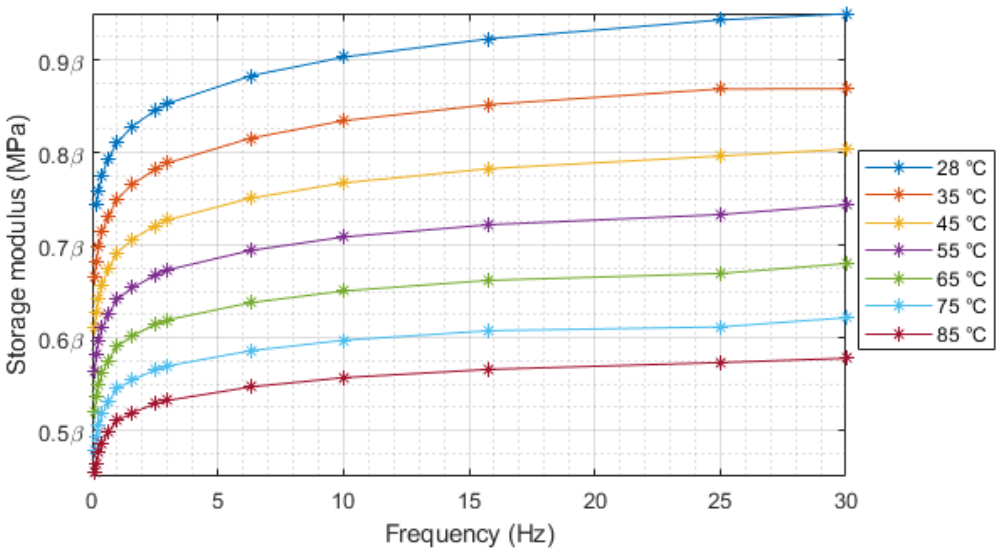

Figure 3: Evolution of the storage modulus depending on the frequency and the temperature.

Viscoelasticity is often modelled by the generalized Maxwell model [3]. Mathematically this model is described by the Prony series, thus the shear relaxation modulus is:

$$G(t) = G_\infty + \sum_i G_i e^{-t/\tau_i} \quad (2)$$

Where G_∞ is the long-term modulus once the material is totally relaxed, τ_i are the relaxation times, and G_i are modulus linked to the associated relaxation times. Prony series can also be expressed in the frequency domain. The storage modulus is established as follow,

$$G'(\omega) = G_\infty + \sum_i \frac{G_i \omega^2 {\tau_i}^2}{1+\omega^2 {\tau_i}^2} \quad (3)$$

Then it's possible to estimate Prony parameters using a curve fitting algorithm [6]. In this study three terms of the series are used. Normalized coefficients g_i are defined as $g_i = G_i/G_0$, with G_0 the relaxation modulus evaluated at $t = 0$. Thus, the Prony series does not depend on temperature. Its fitted coefficients are gathered in Table 2.

g_i	τ_i
0.0664 η	0.015
0.0574 η	0.134
0.0615 η	0.907

Table 2: Fitted Prony coefficients.

3 Experimental characterization

3.1 Experimental set-up

To be able to evaluate the accuracy of the models previously presented, experimental measurements were performed on the first rubber coupling. The secant radial dynamic stiffness is obtained by imposing a radial deflection to the part using a hydraulic shaker capable to develop a force up to 62 kN, while the force is measured using three load cells.

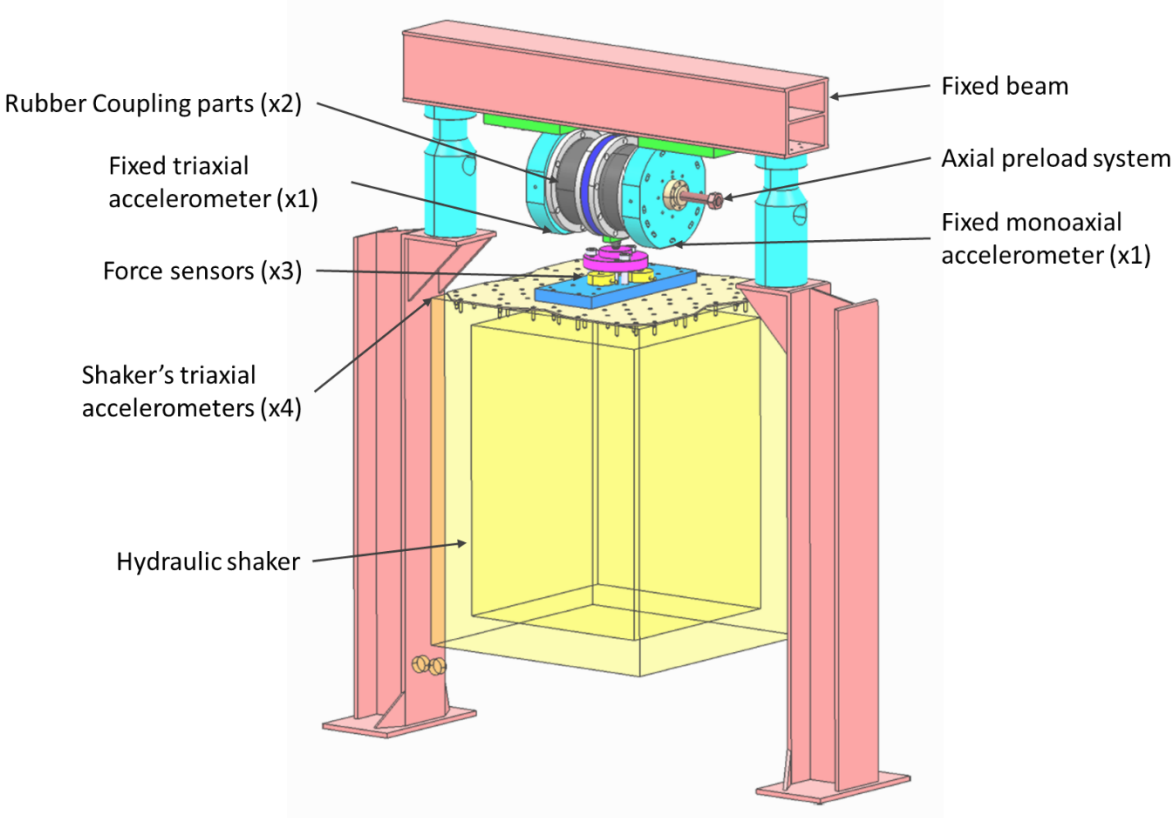

Figure 4: Experimental set-up for the radial test carried out on two identical rubber couplings.

The assembly, presented in Figure 4, is made up of two identical rubber couplings to equilibrate the forces and suppress undesirable bending momentum. A very stiff steel frame is fixed above the shaker to create a reaction support on which it is possible to deform the parts. In addition to the four accelerometers fixed on the top corners of the shaker, other accelerometers were fixed on the reaction support to measure its possible distortion and then achieve the relative rubber deflection. A preload system was also used to apply a static axial preload and study its influence on the radial dynamic properties.

3.2 Results

After postprocessing accelerometers and force sensors signals the force – deflection hysteresis loops are obtained. Figure 5 shows some loops measured for different imposed dynamic amplitudes. As expected, a stiffening is observed when the amplitude is reduced.

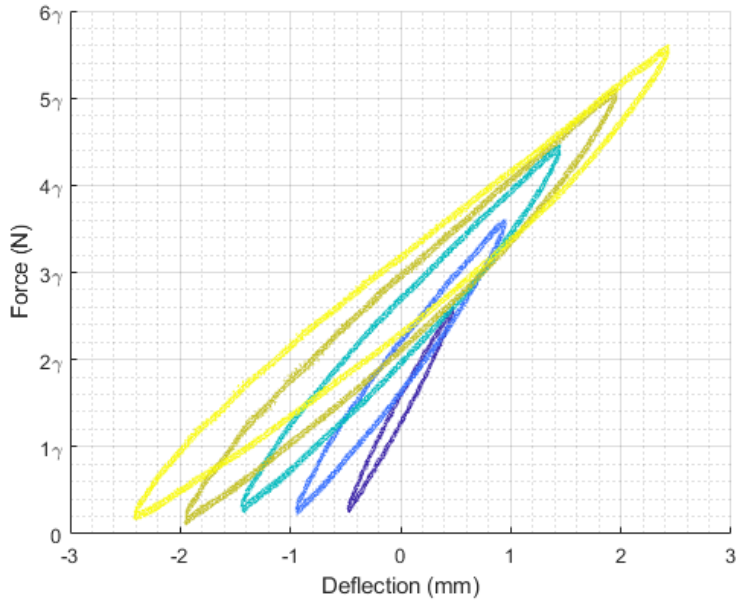

Figure 5: Example of radial force – deflection hysteresis loops obtained for different dynamic amplitudes.

Many tests were performed, for different values of frequency, dynamic amplitude, and axial preload. Figure 6 summarizes the secant stiffness obtained for each set of parameters. The dynamic amplitude and traction preload (+5 mm) have a significant influence on the stiffness. The influence of the frequency must be analysed carefully, especially at low amplitudes, as the results are also influenced by the rubber temperature. In this study it was not possible to control the temperature during the tests, but recordings show an obvious dependency between the imposed displacement frequency and the material temperature.

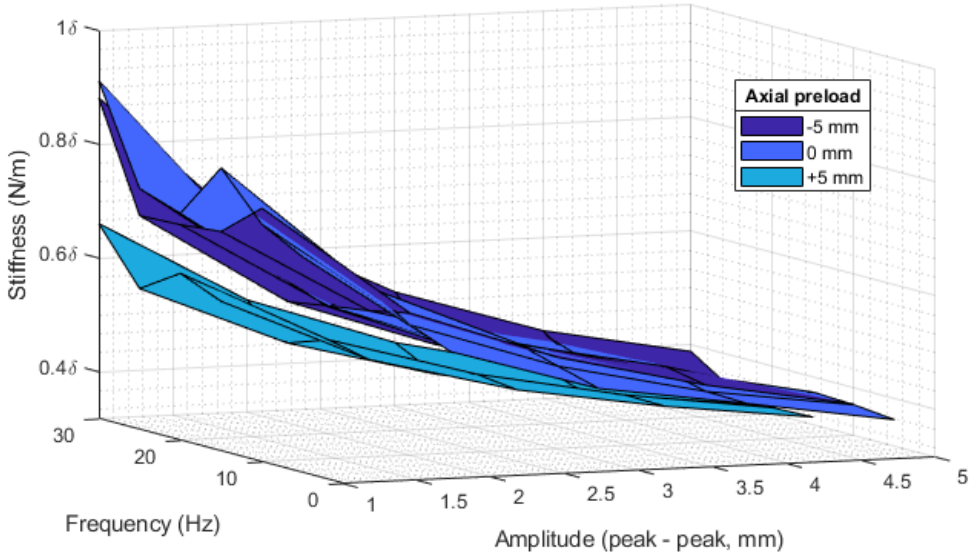

Figure 6: Radial stiffness evolution depending on the axial preload, the dynamic amplitude and frequency.

4 Numerical simulations

4.1 Comparison with the experimental measurements

The experimental tests are now reproduced numerically using Abaqus software with the models described previously for two frequencies (5Hz and 30Hz) and two temperatures (26°C and 65°C), which are the boundary values encountered during the experimentation. Both experimental and numerical results are compared in Figure 7. The influence of temperature is clearly visible: the experimental results at low amplitude are close to the numerical results at low temperature and the experimental results at high amplitude are close to the numerical results at 65°C. The same order of magnitude of temperatures were recorded during the experimentation for the different amplitudes. Thus, the numerical model is considered reliable.

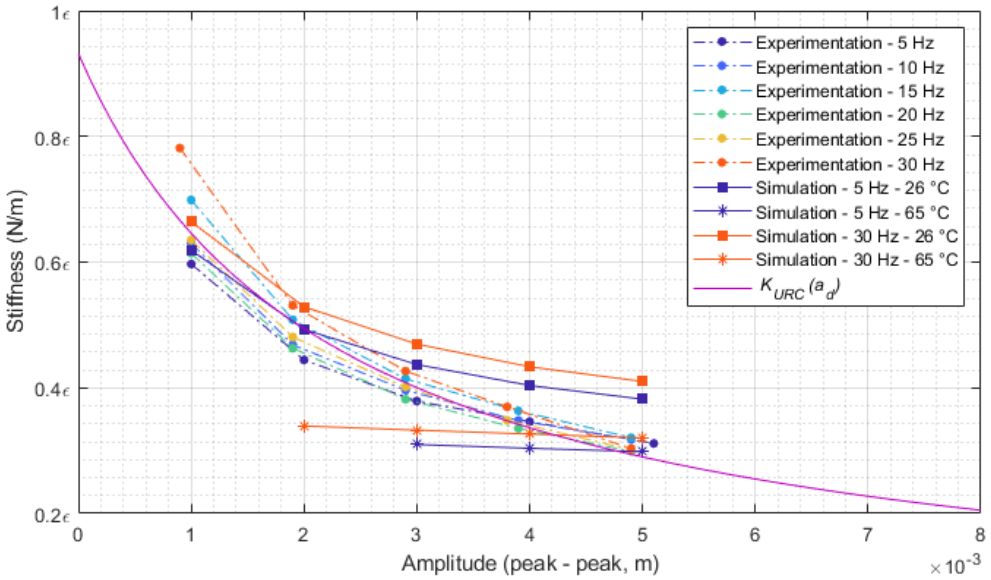

Figure 7: Radial stiffness evolution for the first rubber coupling geometry – experimental, numerical, and analytical results.

In order to implement easily and efficiently this rubber coupling element into the global Finite Elements multirotor model the radial dynamic stiffness is inputted as a simple function $K_{URC}(a_d)$, also represented in Figure 7. The function takes only the dynamic amplitude a_d as parameter: the influence of the frequency is considered negligeable, and the influence of the temperature is considered directly linked to the amplitude.

4.2 Dynamic properties of the second geometry

The second rubber coupling can now be numerically characterized using the same models and parameters, which are now validated. Figure 8 shows the simulation results for the same two frequencies (5Hz and 30Hz) and the same two temperatures (26°C and 65°C), as well as the simple function $K_{MRC}(a_d)$ describing the evolution of the radial stiffness of this second rubber coupling geometry depending on the dynamic amplitude. This time the function $K_{MRC}(a_d)$ is only determined from the numerical results and, as observed in Figure 7, the operational radial stiffness is considered close to the results at 26°C for the smallest amplitudes and close to the results at 65°C for the higher amplitudes.

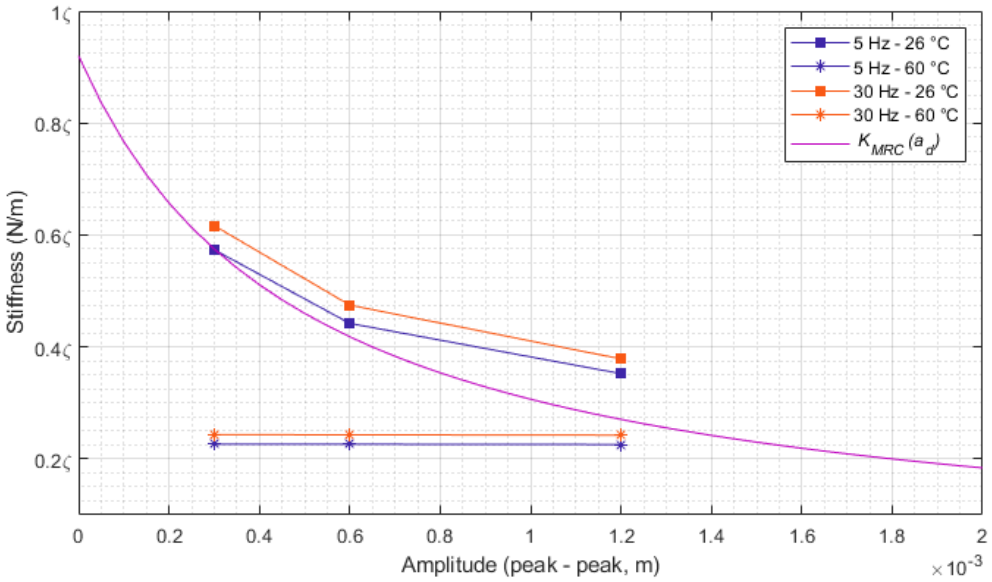

Figure 8: Radial stiffness evolution for the second rubber coupling – numerical results.

5 Conclusion and perspectives

The method presented in this paper is established to predict the radial dynamic stiffness of two rubber coupling parts. The main benefit of the method is that it doesn't require to perform experimentation on rubber coupling having a different design. Indeed, now that the numerical model has been validated it is easy to improve the rubber coupling and once again access its dynamic properties without needing to build and test a new part. It's also possible to change the constitutive material and study the influence on the equivalent dynamic stiffness, only by carrying out new DMA tests.

This method enables to use an accurate and simplified analytic model to describe the dynamic behaviour of a vibration isolator into the Finite Element model of another system, which is significantly reducing the computation time.

Acknowledgments

The authors would like to thank Menard and Vibro Services companies for their financial and technical supports. The authors would also like to thank Franck Legrand, Dr. Florent Dalmas, Pr. Thouraya Nouri Baranger, and Dr. Julien Colmars for their technical support.

The authors are indebted to the French National Research Agency (Funder ID: 10.13039/501100001665) (ANR) for its financial support within the framework of Equipex PHARE 10-EQPX-0043.

References

[1] K. Kirsch and F. Kirsch, *Ground Improvement by Deep Vibratory Methods*, 2nd edn., Boca Raton, USA: CRC Press, 2017.

[2] P. Nagy, Deep Vibro Compaction - Dynamic Compaction Control Based on the Vibrator Movement, PhD thesis, Vienna University of Technology, 2018.

[3] G. Petitet and M. Barquins, *Matériaux caoutchouteux*, Lausanne, Switzerland: PPUR, 2008.

[4] G. Marckmann and E. Verron, *Comparison of hyperelastic models for rubber-like materials*, Rubber Chemistry and Technology, American Chemical Society, 2006, 79 (5), pp.835-858.

[5] G. A. Holzapfel, *Nonlinear Solid Mechanics: A Continuum Approach for Engineering*, Chichester, England: Wiley, 2000.

[6] A. Tapia, L. Lugo, M. Dehonor, *Prony series calculation for viscoelastic behavior modeling of structural adhesives from DMA data*, Ingeniería Investigación y Tecnología, 2020, 21 (2), pp.1-10.